Biosensors and Bioelectronics 41 (2013) 776–782

Contents lists available at SciVerse ScienceDirect

Biosensors and Bioelectronics

journal homepage: www.elsevier.com/locate/bios

# A novel electrochemiluminescence ethanol biosensor based on tris(2,2′-bipyridine) ruthenium (II) and alcohol dehydrogenase immobilized in graphene/bovine serum albumin composite film

Wenhua Gao [a,b,*], Yunsheng Chen [a], Jing Xi [a], Shaoyu Lin [c], Yaowen Chen [b], Yuejuan Lin [b], Zhanguang Chen [a]

[a] Department of Chemistry, Shantou University, Shantou, Guangdong 515063, China
[b] Analysis & Testing Center, Shantou University, Shantou, Guangdong 515063, China
[c] Longhu Environmental Protection Bureau, Shantou, Guangdong 515063, China

ARTICLE INFO

*Article history:*
Received 17 July 2012
Received in revised form
26 September 2012
Accepted 2 October 2012
Available online 11 October 2012

*Keywords:*
Bovine serum albumin
Electrochemiluminescence
Ethanol biosensor
Graphene
$Ru(bpy)_3^{2+}$

ABSTRACT

We developed a novel electrochemiluminescence (ECL) ethanol biosensor based on $Ru(bpy)_3^{2+}$ and alcohol dehydrogenase (ADH) immobilized by graphene/bovine serum albumin composite film. The graphene film was directly formed on a glassy carbon electrode surface via an in situ reduction of graphene oxide (GO) and $Ru(bpy)_3^{2+}$ was immobilized during its formation. The graphene film acted as both a decorating agent for immobilization of $Ru(bpy)_3^{2+}$ and a matrix to immobilize bovine serum albumin (BSA), meanwhile BSA not only acted as a reductant to reduce GO, but also provided a friendly environment for ADH immobilization. Furthermore, ADH was separated from $Ru(bpy)_3^{2+}$ by the electron-conductive graphene/BSA composite film to retain its enzymatic activity. The experimental results indicated that the biosensor had excellent electrochemical activity, ECL response to ethanol and stability. Such a design of $Ru(bpy)_3^{2+}$–graphene/BSA film to modify electrode holds a great promise as a new biocompatible platform for the development of enzyme-based ECL biosensors.



## 1. Introduction

Electrochemiluminescence (ECL) is a process of converting electrochemical energy into radiative energy on the surface of electrode. Among many organic and inorganic ECL systems, ECL based on tris(2,2′-bipyridine) ruthenium(II) [$Ru(bpy)_3^{2+}$] has received considerable attention due to its unique advantages of good electrochemical stability, high ECL efficiency, and the convenience to couple with various separation techniques (Richter, 2004; Miao, 2008). However, many micro-environmental factors in solution, such as viscosity, temperature, surfactant, ion strength and pH would affect the $Ru(bpy)_3^{2+}$ ECL in solution. In addition, the continuous consumption of $Ru(bpy)_3^{2+}$ in solution also limits the widespread application of $Ru(bpy)_3^{2+}$ ECL (Dai et al., 2009). Since $Ru(bpy)_3^{2+}$ can be regenerated during the ECL reaction, ECL sensor, viz. immobilizing $Ru(bpy)_3^{2+}$ on the electrode surface, can not only overcome these problems but also simplify experimental design sensors (Guo et al., 2004; Sun et al., 2007). ECL biosensor based on $Ru(bpy)_3^{2+}$ and enzyme immobilized on the electrode is more suitable for biomolecular sensing with the advantages of ECL sensor (Wei et al., 2007). However, ECL biosensor suffers from the loss of the enzyme activity because the positive charges of $Ru(bpy)_3^{2+}$ could interact with the negative charges of the enzyme (Deng et al., 2009). Many efforts are made to overcome the problem, and the immobilization of the $Ru(bpy)_3^{2+}$ and enzyme by different layers on one electrode has been regarded as one of the best methods. The sol–gel (Deepa et al., 2003), $Ru(bpy)_3^{2+}$–gold nanoparticles (AuNPs) cluster (Zhang et al., 2007) and titania–Nafion composite films (Jia et al., 2009) were applied as the matrix to co-immobilize enzyme and $Ru(bpy)_3^{2+}$ in previous reports. Although the reported ECL biosensors exhibited good performances for the detections, they suffered from slow electron-transfer rate because of the introduction of sol–gel and Nafion hybrid film. Therefore, the development of the highly sensitive ECL biosensor is still drawing much attention. Various nano-materials as excellent electric conductors and favorable platforms for immobilizing $Ru(bpy)_3^{2+}$ and enzymes are being developed, and graphene comes into the picture just in time.

Graphene exhibits unique nanostructure and extraordinary properties (Geim and Novoselov, 2007). Its fame comes to the climax when the Nobel Prize in Physics was awarded to Geim and Novoselov who discovered graphene in 2010. Up to now, graphene has been mainly studied in applications of nanoelectronics

* Corresponding author at: Department of Chemistry, Shantou University, Shantou, Guangdong 515063, China. Tel.: +86 75482902774; fax: +86 75482903941.
*E-mail address:* whgao@stu.edu.cn (W. Gao).

0956-5663/$ - see front matter © 2012 Elsevier B.V. All rights reserved.
http://dx.doi.org/10.1016/j.bios.2012.10.005

(Roche, 2011), solar cells (Wang et al., 2008), and supercapacitors (Wang et al., 2009a). Moreover, its analytical applications are being explored. As an excellent electric conductor, graphene has been employed in many schemes for electrochemistry analysis (Wang et al., 2011). Because of high surface area, high π-conjunction and hydrophobic properties, graphene can provide a platform for immobilizing organic and inorganic molecules (Wang et al., 2012; Kuila et al., 2011). In addition, graphene has been studied in the chemiluminescence (CL) detection because of its excellent optical transmittance (Lv et al., 2009). Considering the excellent properties of graphene, we believe that graphene can be competent to act as an attractive matrix for the fabrication of ECL biosensor. Up to now, graphene was distributed in the Nafion composite film to transfer electron. However, the sensor based on $Ru(bpy)_3^{2+}$ immobilized by graphene–Nafion film suffered from slow electron-transfer rate due to the introduction of Nafion (Li et al., 2009). Graphene oxide (GO), different from graphene, was also used to fabricate the ECL sensor for its oxygen functional groups. However, this approach was limited by expensive reagents and complex operations of derivation (Chen et al., 2010). Furthermore, graphene, different from graphene oxide (GO), has not been tried in the fabrication of ECL biosensor based on immobilizing both Ru(II) complexes and enzyme.

In our previous work, we discovered that $Ru(bpy)_3^{2+}$ was immobilized during the formation of graphene film on the glassy carbon electrode (GCE) surface via the in situ wet-chemical reduction of GO (Gao et al., 2012). In particular, bovine serum albumin (BSA) can reduce GO at a suitable pH and reaction temperature, and then adhere to the surface of graphene due to the interaction of the remaining epoxy groups on graphene and amino groups on BSA (Liu et al., 2010; Ji et al., 2013). Other than the immobilization of $Ru(bpy)_3^{2+}$, enzymatic catalytic activity is an important factor that affects the ECL biosensor performance. Enzyme can be immobilized on the electrode by a cross-linking procedure using glutaraldehyde (GA), which has been used in the fabrication of enzyme-based biosensors. Since the lysine groups are present in its structure, BSA can provide a friendly environment for enzyme immobilization, which endows the enzyme greater activity than with direct enzyme immobilization without BSA (Crespilho et al., 2009). Herewith, we described an approach to fabricate an ECL ethanol biosensor based on $Ru(bpy)_3^{2+}$ and enzyme immobilized by graphene/BSA composite film. In this ECL biosensor, graphene formed on the surface of GCE can act as a decorating agent to immobilize $Ru(bpy)_3^{2+}$ and BSA, while BSA not only acted as a reductant to reduce GO, but also provided a friendly environment for enzyme immobilization. Furthermore, enzyme was separated from $Ru(bpy)_3^{2+}$ by the electron-conductive graphene/BSA composite film to retain its enzymatic activity. With alcohol dehydrogenase (ADH) as a model, we then constructed an ECL ethanol biosensor.

## 2. Experimental

### 2.1. Chemicals

Alcohol dehydrogenase (ADH) (EC 1.1.1.1, from baker's yeast, 300 units/mg solid), nicotinamide adenine dinucleotide ($NAD^+$) (sodium salt, from yeast), Tris(2,2-bipyridyl) dichlororutheniu-m(II) hexahydrate [$Ru(bpy)_3Cl_2 \cdot 6H_2O$], BSA were purchased from Sigma-Aldrich (St. Louis, MO, USA). Ethanol, ammonia, sodium dihydrogen phosphate and GA were purchased from Sinopharm Chemical Reagent Co. Ltd. (Shanghai, China). All other chemicals were of analytical grade. All solutions were prepared with deionized water obtained from a Milli-Q water purification system (Bedford, MA, USA). All measurements were carried out at room temperature, $24 \pm 2$ °C.

### 2.2. Apparatus

Cyclic voltammetry (CV) curves were measured with IM6ex electrochemical workstation (Zahner IM6ex, Germany). ECL detections were carried out with an MPI-B capillary electrophoresis ECL detector and the negative high voltage of −800 V was applied to power the photomultiplier tube (PMT) (Remax, China). A GCE (3 mm in diameter) coated with $Ru(bpy)_3^{2+}$–graphene/BSA/ADH film, an Ag/AgCl (1 M KCl) electrode, and a platinum wire were used as working, reference, and counter electrode in this work, respectively. UV–vis spectra were obtained on a Lambda 950 spectrophotometer (Perkin Elmer, USA). Atomic force microscopy (AFM) was performed on a Digital Instruments Nanoscope IIIa (Veeco, CA). Scanning electron microscope (SEM) and energy-dispersive spectroscopy (EDS) were carried out on a JSM-6360LA (JEOL, Japan). A PHS-3CA precision pH meter (Dapu, China) was used in the experiment. Raman spectra were recorded on a Jobin Yvon LABRAM-HR confocal laser micro-Raman spectrometer (Jobin Yvon,

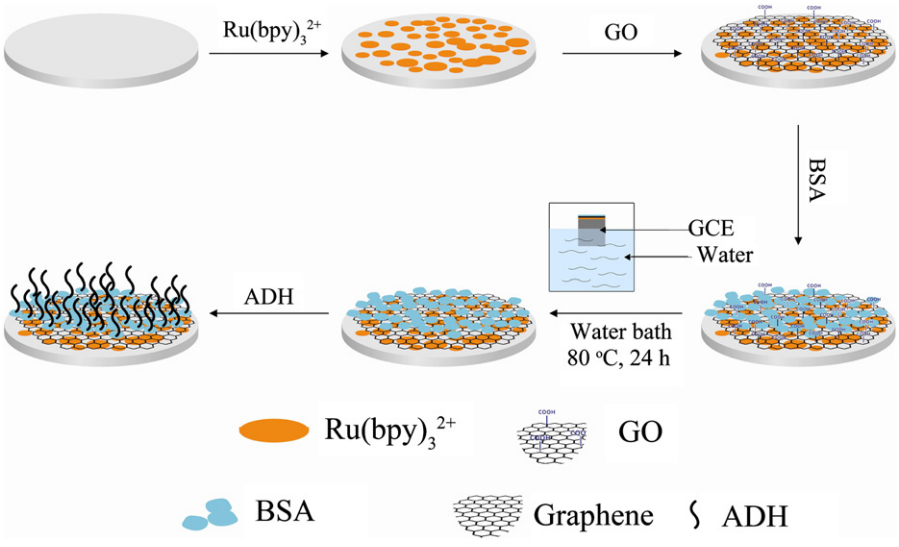


**Fig. 1.** Formation of ECL ethanol biosensor based on graphene/BSA composite film.

France) at room temperature and an excitation wavelength of 514.5 nm.

### 2.3. Preparation of the ECL ethanol biosensor

GO was prepared from graphite flake based on the Hummers method. Before being modified, GCE was polished using alumina slurry (0.05 μm) on a polishing cloth, and then sonicated in deionized water and anhydrous ethanol respectively. As shown in Fig. 1, the fabrication of ECL ethanol biosensor was described as follows. Firstly, 10 μL 2 mg/mL $Ru(bpy)_3^{2+}$ homogeneous solution was dropped on the clean GCE surface and then dried under ambient condition. Secondly, 10 μL 1 mg/mL GO homogeneous solution was dropped and the $Ru(bpy)_3^{2+}$ film was covered. Thirdly, after the GO solution dried in the air, a 10 μL reductant containing 0.6 mg/ml BSA and 200 mM ammonia solution was dropped, and then the electrode was put in a closed water-bath system at 80 °C to keep a very wet environment. To form a firm graphene film, the reduction reaction went on slowly in wet environment for 24 h. Third, after the reductant drying, the electrode was carefully washed to remove the loose $Ru(bpy)_3^{2+}$ and unfixed graphene aggregations with deionized water. Successively, 10 μL of the mixture of 1 mg/mg ADH and 40 mM GA (2:1, v/v) was dropped on the dried electrode and dried at 4 °C. Finally, the modified GCE was carefully washed with deionized water, and then the ECL ethanol biosensor was obtained.

## 3. Results and discussion

### 3.1. Characterization of the ECL ethanol biosensor

A successful reduction of GO to graphene by BSA was verified by UV–vis and Raman spectroscopy. In this process, 10 μL GO solution and 10 μL reductant were well mixed and dried in air. The dried graphene was used for UV–vis and Raman measurements. Fig. 2A shows the UV–vis spectra of GO solution (Curve a) and graphene dispersive solution (Curve b). The absorption peak of GO around 230 nm was red-shifted towards 260 nm after reaction, indicating that GO had been directly reduced by BSA on the GCE surface. Furthermore, the Raman spectra of GO film (Curve a) and graphene film (Curve b) both exhibited typical features which were D band at 1344 $cm^{-1}$ and G band at 1596 $cm^{-1}$ as shown in Fig. 2B. The D band arose from $sp^3$ hybridized carbon, and the G band represented the $E_{2g}$ zone center mode of the crystalline graphite, and the intensity ratio of D band to G band ($I_D/I_G$) was proportional to the number of defect sites in graphite carbon (Zhou et al., 2009). $I_D/I_G$ slightly increased from 0.953 to 1.14 after the reduction, so we could draw conclusions as follows: firstly, GO had been reduced to graphene already (Wang et al., 2009b). Secondly, the reduction process did not reduce the size of in-plane $sp^2$ domains greatly, which was favorable to the electro-conductivity of graphene film (Guo et al., 2010). In conclusion, these results demonstrated that the well electro-conductive graphene/BSA composite film could be formed on the GCE surface.

The taping mode AFM and SEM was used to describe the change on the electrode surface. The samples were prepared as mentioned in Section 2.2. Fig. 3A shows the images of $Ru(bpy)_3^{2+}$–GO film. Fig. 3B and C shows the image of the $Ru(bpy)_3^{2+}$–GO/BSA before and after undergoing the reduction reaction respectively. Fig. 3D shows the surface of the ECL ethanol biosensor. Compared with Fig. 3A, $Ru(bpy)_3^{2+}$–GO/BSA had been thicker from 0.85 nm to 1.7 nm. Moreover, the roughness of $Ru(bpy)_3^{2+}$–GO/BSA was also increased. The phenomenon was a strong indicator that BSA uniformly spread onto GO sheet. In a comparison between Fig. 3B and Fig. 3C, the $Ru(bpy)_3^{2+}$–GO/BSA was thinner when the reduction finished. The result could be explained as that the oxygen functional groups on GO had decreased after reacting with BSA (Geng et al., 2010; Chen et al., 2001). Meanwhile, the $Ru(bpy)_3^{2+}$–graphene/BSA was also thicker than $Ru(bpy)_3^{2+}$–GO, indicating that BSA still uniformly spread onto graphene sheet. Such unique structure provided a friendly environment for ADH immobilization. As shown in Fig. 3D, the thickness of ECL ethanol biosensor notably increased, which implies the BSA on graphene could provide a large amount of conjugate sites to ADH. Furthermore, the morphologies of four steps were also observed by SEM. The morphologies of $Ru(bpy)_3^{2+}$–GO film, $Ru(bpy)_3^{2+}$–GO/BSA before and after undergoing the reduction reaction and the ECL ethanol biosensor were correspondingly shown in Fig. 4A, B, C and D. Compared to Fig. 4A, Fig. 4B showed the $Ru(bpy)_3^{2+}$–GO/BSA can form a uniform film from lamellar structures. After reduction reaction, the film became finer and more uniform (Fig. 4C). With the addition of ADH, the film

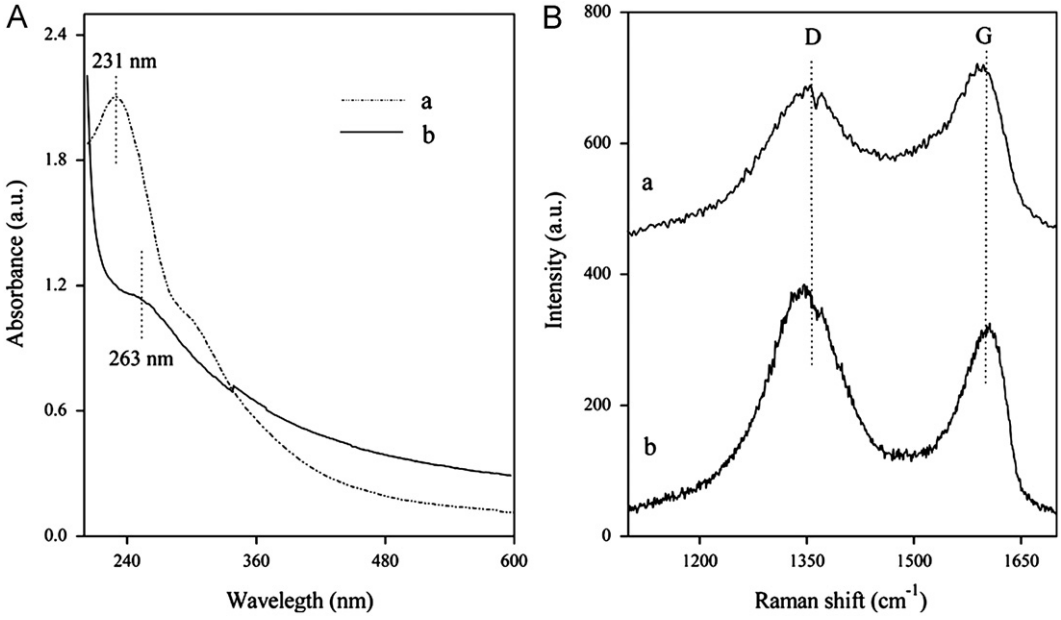


**Fig. 2.** (A) UV–vis spectra of GO (Curve a) and graphene dispersive solution (Curve b); (B) Raman spectra of GO (Curve a) and graphene film (Curve b).

became microscopically rougher. The AFM and SEM results indicated that the $Ru(bpy)_3^{2+}$–graphene/BSA film and ADH can be immobilized on the GCE surface.

The EDSs confirm the atomic ratio of Ru/C to reveal that the $Ru(bpy)_3^{2+}$ contents on the surface of $Ru(bpy)_3^{2+}$–GO film (Fig. S1A) and graphene/BSA composite film (Fig. S1B) on silicon wafer. It could be found that the ratio of Ru/C had a drastic reduction from 0.02 to 0.004, which demonstrated that little $Ru(bpy)_3^{2+}$ existed on the surface of graphene/BSA composite film. Therefore, such unique structure could effectively separate $Ru(bpy)_3^{2+}$ from ADH, which could greatly decrease the impact of positive charges of $Ru(bpy)_3^{2+}$ on the enzymatic activity.

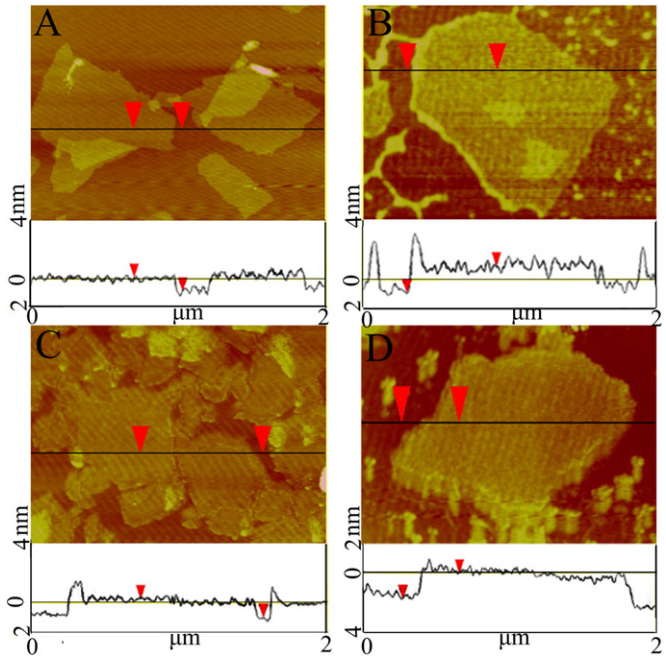


**Fig. 3.** AFM images of $Ru(bpy)_3^{2+}$–GO sheet (A); $Ru(bpy)_3^{2+}$–GO/BSA (B); $Ru(bpy)_3^{2+}$–graphene/BSA (C); $Ru(bpy)_3^{2+}$–graphene/BSA/ADH (D) on mica.

### 3.2. Optimization of experimental variables

Since BSA could co-react with $Ru(bpy)_3^{2+}$ and produce ECL signal, an excess BSA affected the determination of the ethanol and increased the barrier for electron-transfer. Insufficient BSA affects the reduction of GO, which affected the immobilization of the $Ru(bpy)_3^{2+}$. Therefore, the optimal amount of BSA was chosen by the difference of ECL intensity ($\Delta_{ECL}$) between the absence and presence of 500 μM ethanol in 100 mM phosphate buffer solution (PBS, pH 7.0) with 1.0 mM $NAD^+$. As shown in Fig. S2A, the largest $\Delta_{ECL}$ indicated that the biosensor had the largest response to ethanol when the BSA was 0.6 mg/mL in reductant. When BSA was less than 0.6 mg/ml, $\Delta_{ECL}$ increased with the increasing BSA because more GO was reduced and more $Ru(bpy)_3^{2+}$ was immobilized. However, when BSA was more than 0.6 mg/ml, $\Delta_{ECL}$ decreased sharply with the increasing BSA. The phenomenon could be explained as follows: firstly, BSA reacted with $Ru(bpy)_3^{2+}$ prior to NADH. Secondly, further increase in the amount of BSA in electrode might be leading to the increase of the diffusional barrier for the electron-transfer from NADH to $Ru(bpy)_3^{2+}$. Therefore, 0.6 mg/mL BSA in reductant was chosen.

As a necessary cofactor in dehydrogenase-based ECL biosensor, $NAD^+$ was added into PBS. The following schemes demonstrated how $Ru(bpy)_3^{2+}$ ECL can be coupled with $NAD^+$ recycling with ADH (Jameison et al., 1996; Xu et al., 2005):

$$Ru(bpy)_3^{2+} - e^- \rightarrow Ru(bpy)_3^{3+} \quad (1)$$

$$alcohol + NAD^+ \xrightarrow{ADH} acetaldehyde + NADH + H^+ \quad (2)$$

$$Ru(bpy)_3^{3+} + NADH \rightarrow Ru(bpy)_3^{2+*} + NAD^+ \quad (3)$$

$$Ru(bpy)_3^{2+*} \rightarrow Ru(bpy)_3^{2+} + h\nu \quad (4)$$

The effect of $NAD^+$ concentration on the ECL ethanol biosensor response was examined in 100 mM PBS (pH 7.0) with 500 μM ethanol. As shown in Fig. S2B, the biosensor response increased as the amount of $NAD^+$ increased up to 1.0 mM. When the amount of $NAD^+$ further increased, the ECL response decreased slightly. The increased ECL response can be attributed to more efficient enzymatic reaction with higher concentration of $NAD^+$ (Appelqvist et al., 1985).

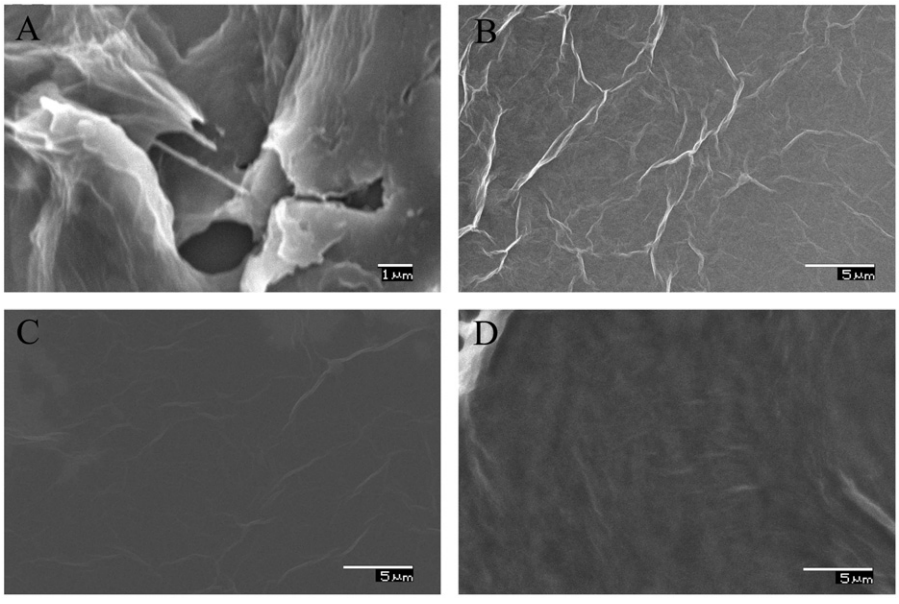


**Fig. 4.** SEM images of $Ru(bpy)_3^{2+}$–GO sheet (A); $Ru(bpy)_3^{2+}$–GO/BSA (B); $Ru(bpy)_3^{2+}$–graphene/BSA (C); $Ru(bpy)_3^{2+}$–graphene/BSA/ADH (D).

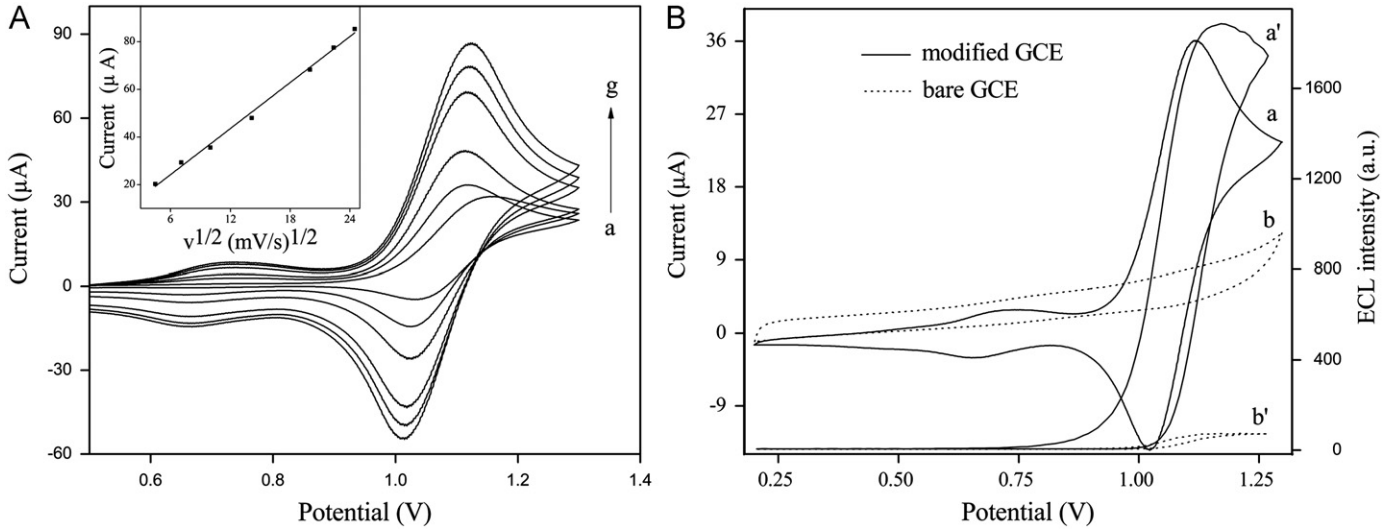


**Fig. 5.** (A) The CVs of the biosensor at the different scan rate in 100 mM PBS (pH 7.0). a–g Correspond to scan rate: 20, 60, 100, 200, 400, 500 and 600 mV/S respectively. (B) CVs of 100 mM PBS (pH 7.0) on the bare GCE (Curve b) and the ECL ethanol biosensor (Curve a), and ECL–potential curve of bare GCE (Curve b′) and the ECL ethanol biosensor (Curve a′) to 500 μM ethanol. Scan rate: 100 mV/s.

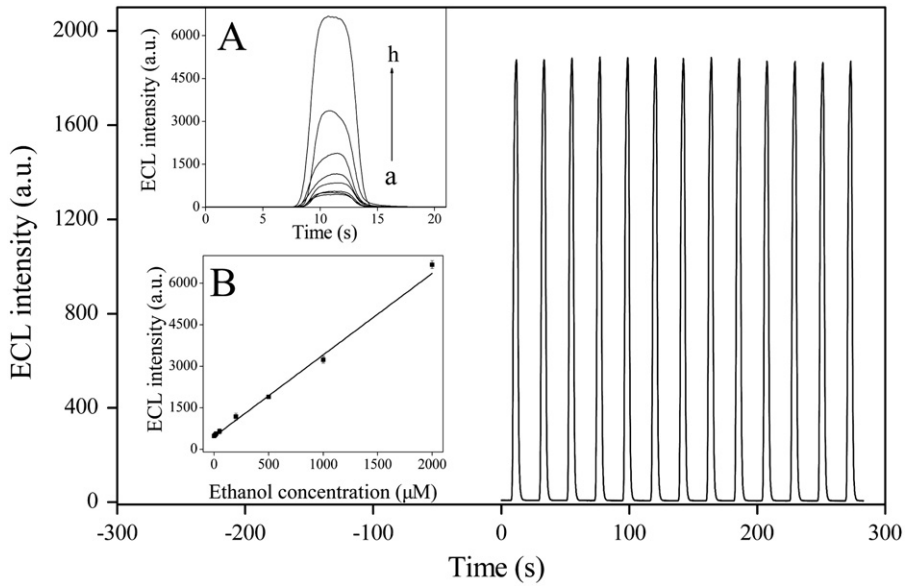


**Fig. 6.** ECL response from the ethanol biosensor in 100 mM PBS (pH 7.0) containing 1.0 mM $NAD^+$ and 500 μM ethanol under continuous CVs from 0.2 V to 1.3 V. Scan rate: 100 mV/s. Inset A: The ECL intensity of the biosensor with different ethanol concentrations (from a to h: 1, 10, 20, 50, 200, 500, 1000 and 2000 μM, respectively). Inset B: calibration curve for ethanol of the biosensor in 100 mM PBS (pH 7.0) containing 1.0 mM $NAD^+$. Error bars show standard deviations ($n=3$).

Therefore, the $NAD^+$ cofactor of 1.0 mM was used in all the experiments.

### 3.3. Electrochemistry and ECL behaviors of the ECL ethanol biosensor

Fig. 5A shows CVs of the ECL ethanol biosensor in 100 mM PBS (pH 7.0) at different scan rates. A pair of redox wave characteristics of $Ru(bpy)_3^{2+}$/$Ru(bpy)_3^{3+}$ appeared. As shown in the inset of Fig. 5A, the anodic peak current was proportional to the square root of the scan rate over the range of 20–600 mV/s, indicating that the immobilized $Ru(bpy)_3^{2+}$ underwent a diffusion process and the biosensor had an excellent electron transfer rate.

The electrochemistry behavior was studied in 100 mM PBS (pH 7.0) at 100 mV/s from 0.2 to 1.3 V. As shown in Fig. 5B, no visible electrochemical response was obtained on the bare GCE (Curve b). The CV of the biosensor (Curve a) showed a pair of quasi-reversible redox peaks with a peak separation of 0.13 V due to the electrochemical transition between $Ru(bpy)_3^{2+}$ and $Ru(bpy)_3^{3+}$. Furthermore, an oxidation peak at 1.14 V and a reduction peak at 1.01 V corresponded with the electrochemistry behavior of $Ru(bpy)_3^{2+}$ in PBS, which indicated that $Ru(bpy)_3^{2+}$ was immobilized by graphene/BSA–ADH film. Meanwhile, higher anodic current of oxidation peak in Curve a was observed in comparison to Curve b, demonstrating that the biosensor had excellent electrochemical activity. Furthermore, the surface coverage ($\Gamma$) of $Ru(bpy)_3^{2+}$ on the biosensor could be calculated using Faraday's law, that is, $\Gamma = Q/nFA$, where $Q$ is the charge consumed in the reaction and is obtained by integrating the anodic peak of the CV at 100 mV $s^{-1}$, $n$ is the number of electrons involved in the oxidation, $F$ and $A$ stand for the Faraday constant and the electroactive surface area of the electrode ($cm^{-2}$), respectively (Vase et al., 2007). $\Gamma$ was found to be $2.35 \times 10^{-8}$ mol $cm^{-2}$ in the current study.

The ECL behavior was researched in 100 mM PBS (pH 7.0) with 1.0 mM $NAD^+$ and 500 μM ethanol at 100 mV/s from 0.2 to 1.3 V.

The ECL–potential curve displayed the ECL behaviors of the ECL ethanol biosensor as shown in Fig. 5B. As shown in Curve b′, there was no ECL response on bare GCE. The ECL ethanol biosensor has obvious ECL response to ethanol (Curve a′), which also corresponded with the ECL behavior of $Ru(bpy)_3^{2+}$. This result of ECL behaviors demonstrated that the ECL ethanol biosensor had an excellent response to ethanol.

### 3.4. ECL ethanol biosensor for ethanol

This unique immobilization method led to a strong ECL response to ethanol. The calibration plot for alcohol detection with the ECL ethanol biosensor under optimal experimental conditions was also studied. Inset A of Fig. 6 shows ECL intensity with different concentrations of alcohol. Inset B of Fig. 6 shows the calibration curve. It was observed that the ECL intensity presented a good linearity with the ethanol concentrations ranging from 1 to 2000 μM. The regression equation is $I=(461.9\pm21.9)+(2.947\pm0.052)\,C$ ($n=8$) with a correlation coefficient ($r$) of 0.9962, where $I$ is the ECL intensity and $C$ is the ethanol concentration (μM). The limit of detection (LOD), calculated as the blank plus three times the standard deviation (Duan et al., 2010), was found to be 0.1 μM, which was three orders lower than that at the Nafion-sol–gel hybrid film-modified electrode (Xu et al., 2005), two orders lower than that at the $Ru(bpy)_3^{2+}$–AuNPs aggregates modified electrode (Zhang et al., 2007), one order lower than that at sol–gel titania–Nafion–MWNT composite film modified electrode (Choi et al., 2007). The improved sensitivity could be explained as follows. Firstly, the graphene/BSA composite film had fast electron-transfer rate because of the absence of traditional auxiliary mediums (such as Nafion and SiNPs). Secondly, ADH had excellent enzymatic catalytic activity with the presence of BSA, which greatly increased the ECL response to ethanol. Moreover, the stability of this biosensor was studied. Under continuous potential scanning for 13 cycles in 100 mM PBS (pH 7.0) with 500 μM ethanol and 1.0 mM $NAD^+$, there was no obvious reduction of ECL intensity as demonstrated in Fig. 6, and the relative standard deviation of ECL was 0.5015%. The long-term stability of the biosensor was also investigated during two weeks by monitoring its ECL response to 500 μM ethanol every two days. The biosensor was stored in a refrigerator at 4 °C between measurements. The ECL intensity gradually decreased to approximately 90% of its initial value within a month (the detail is shown in Table S1). Compared to the biosensors based on silica nanoparticles (Jia et al., 2009) and sol–gel hybrid material (Deng et al., 2009), this biosensor had a better stability. Moreover, the electrode-to-electrode reproducibility was determined at three independently fabricated ECL biosensors. This series yielded a RSD of 9.73%. Two reasons were considered to explain the excellent stability of this ECL biosensor. Firstly, $Ru(bpy)_3^{2+}$ was adsorbed in the basal plane of graphene and prevented from transferring into solution, which made the ECL ethanol biosensor have a well stability. Secondly, ADH was separated from $Ru(bpy)_3^{2+}$ by the electron-conductive graphene/BSA composite film to retain its enzymatic activity.

## 4. Conclusion

In the present work, we developed a novel ECL ethanol biosensor based on $Ru(bpy)_3^{2+}$ and ADH immobilized by graphene/BSA composite film for the first time. The graphene film was directly formed on a GCE surface via an in situ reduction of GO with BSA and immobilization of $Ru(bpy)_3^{2+}$ was completed simultaneously during its formation. The graphene film acted as both a decorating agent for immobilization of $Ru(bpy)_3^{2+}$ and a matrix to immobilize BSA, meanwhile BSA not only acted as a reductant to reduce GO, but also provided a friendly environment for ADH immobilization. Furthermore, ADH was separated from $Ru(bpy)_3^{2+}$ by the electron-conductive graphene/BSA composite film to retain its enzymatic activity. The experimental results indicated that the biosensor had excellent electrochemical activity, ECL response to ethanol and stability. Such a design of $Ru(bpy)_3^{2+}$–graphene/BSA film to modify electrode holds a great promise as a new biocompatible platform for the development of enzyme-based ECL biosensors. Recently, an electrochemical co-assembly approach to immobilize the Ru(II) reagents has been developed (Ji et al., 2013). This approach brings another new dimension in fabricating ECL sensors. Therefore, further experiments, such as improving the ECL sensors via developing new methods to immobilize $Ru(bpy)_3^{2+}$, are on the way.

## Acknowledgments

We acknowledge the financial support of this work by Research Start-up Funding of the Shantou University (no. NTF10002), the Natural Science Foundation of Guangdong Province (no. S2011010005208) and the Science & Technology Project of Guangdong Province (nos. 2010A080403003 and 2011B090400280). We would like to thank Dr. Hualin Fu and Mr. Ping Lan for their support.

## Appendix A. Supporting information

Supplementary data associated with this article can be found in the online version at http://dx.doi.org/10.1016/j.bios.2012.10.005.

## References

Appelqvist, R., Marko-Varga, G., Gorton, L., Torstensson, A., Johansson, G., 1985. Analytica Chimica Acta 169, 237–247.
Chen, R.J., Zhang, Y.G., Wang, D.W., Dai, H.J., 2001. Journal of the American Chemical Society 123, 3838–3839.
Chen, X.M., Wu, G.H., Chen, J.M., Jiang, Y.Q., Chen, G.N., Oyama, M., Chen, X., Wang, X.R., 2010. Biosensors and Bioelectronics 26, 872–876.
Choi, H.N., Yoon, S.H., Lyu, Y.K., Lee, W.Y., 2007. Electroanalysis 19, 459–465.
Crespilho, F.N., Esteves, M.C., Sumodjo, P.T.A., Podlaha, E.J., Zucolotto, V., 2009. Journal of Physical Chemistry C 113, 6037–6041.
Dai, H., Wang, Y.M., Wu, X.P., Zhang, L., Chen, G.N., 2009. Biosensors and Bioelectronics 24, 1230–1234.
Deepa, P.N., Kanungo, M., Claycomb, G., Sherwood, M.A., Collinson, M.M., 2003. Analytical Chemistry 75, 5399–5405.
Deng, L., Zhang, L.H., Shang, L., Guo, S.J., Wen, D., Wang, F., Dong, S.J., 2009. Biosensors and Bioelectronics 24, 2273–2276.
Duan, R.X., Zhou, X.M., Xing, D., 2010. Analytical Chemistry 82, 3099–3103.
Gao, W.H., Chen, Y.S., Xi, J., Zhang, A., Chen, Y.W., Lu, F.S., Chen, Z.G., 2012. Sensors & Actuators B: Chemical 171–172, 1159–1165.
Geim, A.K., Novoselov, K.S., 2007. Nature Materials 6, 183–191.
Geng, X.M., Niu, L., Xing, Z.Y., Song, R.S., Liu, G.T., Sun, M.T., Cheng, G.S., Zhong, H.J., Liu, Z.H., Zhang, Z.J., Sun, L.F., Xu, H.X., Lu, L., Liu, L.W., 2010. Advanced Materials 22, 638–642.
Guo, S.J., Wen, D., Zhai, Y.M., Dong, S.J., Wang, E.K., 2010. ACS Nano 4, 3959–3968.
Guo, Z.H., Shen, Y., Wang, M.K., Zhao, F., Dong, S.J., 2004. Analytical Chemistry 76, 184–191.
Jameison, F., Sanchez, R.I., Dong, L., Leland, J.K., Yost, D., Martin, M.T., 1996. Analytical Chemistry 68, 1298–1302.
Ji, S.B., Yan, Z.H., Wu, J.W., Chen, L.L., Li, H., 2013. Biosensors & Bioelectronics 39, 106–110.
Jia, T.T., Cai, Z.M., Chen, X.M., Lin, Z.J., Huang, X.L., Chen, X., Chen, G.N., 2009. Biosensors & Bioelectronics 25, 263–267.
Kuila, T., Bose, S., Khanra, P., Mishra, A.K., Kim, N.H., Lee, J.H., 2011. Biosensors & Bioelectronics 26, 4637–4648.
Li, H.J., Chen, J., Han, S., Niu, W.X., Liu, X.Q., Xu, G.B., 2009. Talanta 79, 165–170.
Liu, J.B., Fu, S.H., Yuan, B., Li, Y.L., Deng, Z.X., 2010. Journal of the American Chemical Society 132, 7279–7281.
Lv, X., Huang, Y., Liu, Z.B., Tian, J.G., Wang, Y., Ma, Y.F., Liang, J.J., Fu, S.P., Wan, X.J., Chen, Y.S., 2009. Small 5, 1682–1687.
Miao, W., 2008. Chemical Reviews 108, 2506–2553.

Richter, M.M., 2004. Chemical Reviews 104, 3003–3036.
Roche, S., 2011. Nature Nanotechnology 6, 8–9.
Sun, X.P., Du, Y., Zhang, L.X., Dong, S.J., Wang, E.K., 2007. Analytical Chemistry 79, 2588–2592.
Vase, K.H., Holm, A.H., Norrman, K., Pedersen, S.U., Daasbjerg, K., 2007. Langmuir 23, 3786–3793.
Wang, K., Liu, Q., Guan, Q.M., Wu, J., Li, H.N., Yan, J.J., 2011. Biosensors & Bioelectronics 26, 2252–2257.
Wang, X., Zhi, L.J., Müllen, K., 2008. Nano Letters 8, 323–327.
Wang, X.S., Yang, D.P., Huang, G.S., Huang, P., Shen, G.X., Guo, S.W., Mei, Y.F., Cui, D.X., 2012. Journal of Materials Chemistry 22, 17441–17444.
Wang, Y., Shi, Z.Q., Huang, Y., Ma, Y.F., Wang, C.Y., Chen, M.M., Chen, Y.S., 2009a. Journal of Physical Chemistry C 113, 13103–13107.
Wang, Z.J., Zhou, X.Z., Zhang, J., Boey, F., Zhang, H., 2009b. Journal of Physical Chemistry C 113, 14071–14075.
Wei, H., Du, Y., Kang, J.Z., Wang, E.K., 2007. Electrochemistry Communications 9, 1474–1479.
Xu, Z.A., Guo, Z.H., Dong, S.J., 2005. Biosensors & Bioelectronics 21, 455–461.
Zhang, L., Xu, Z., Sun, X., Dong, S.J., 2007. Biosensors & Bioelectronics 22, 1097–1100.
Zhou, M., Zhai, Y.M., Dong, S.J., 2009. Analytical Chemistry 81, 5603–5613.